HIRDLS

TC	OXF	97	A

HIGH RESOLUTION DYNAMICS LIMB SOUNDER

Originator: C. W. P. Palmer

Date: 10th April 1995

Subject/title: RADMETAC Budget Description

This document describes the theory behind the budget allocations in the in-flight radiometric accuracy budget RADMETAC, one of the SPRAT budgets (TC-HIR-57). It consists mainly of the text of a paper to be published by C. W. P. Palmer and J. G. Whitney, but also includes additional notes, and a copy of the channel-dependent budget table.

Key words: Calibration, IFC, Budgets, Radiometric, Scan

Reviewed by:

Approved by:

Oxford University
Department of Atmospheric, Oceanic and Planetary Physics
Clarendon Laboratory
Oxford OX1 3PU, U.K.

EOS

1. Introduction and Scope

This document consists of four parts:

(a) The paper "The Radiometic Calibration Budget for the High Resolution Dynamics Limb Sounder" by C W P Palmer and J G Whitney, to be published in Journal of Atmospheric and Oceanic Technology, which explains the origin of every entry in the RADMETAC budget. A PostScript file of the text is in eos/palmer/radmetac_paper.ps, and on ISAMS in WK1:[PALMER]CAL_PAPER.PS

(b) These notes, which make explicit the assumptions in the budget allocations, and summarize the status of any uncertain items requiring confirmation or further analysis.

(c) The Budget Table itself, which exists as a text file, currently in eos/palmer/radmetac_table.out or USER:[PALMER.HIRDLS]RADMETAC.OUT. Note that this file is 132 columns wide and must therefore be printed either in compressed font or /LANDSCAPE

(d) The IDL program which creates the budget, currently in USER:[PALMER.HIRDLS]RADMETAC.PRO This part is only required for reference, and is not distributed with the remainder of the document.

2. Line Items: Details and Status

No.	Source	Details	S/S	Status
0	IFC BB temperature error	70mK error, to include cal, temp uniformity, offsets, stability to EOL.	IFC/CAL	Apply reqmt to s/s
1	IFC mirror temp. error	IFC paraboloid T error 0.25K based on emissivity 0.03	IFC	Apply reqmt to s/s
2	IFC BB/mirror temp. diff	Max 1K T diff BB/paraboloid, error in emissivity 0.01	IFC/CAL	Apply reqmt to s/s
3	Deficit IFC BB emissivity	effective emissivity 0.997 includes some stray light	IFC	Analysis required
4	Radiometric offset change	Rate of change of telescope chopper and chopper relay mirrors 5 mK in 10 s	TEL	Apply reqmt to s/s
5	Gain stability	Rate of change of gain 2.e-4 in 10s, to include chopping efficiency, throughput, det responsivity, electronic gain	TEL/DET/ SPU	Apply reqmt to s/s
6	Spectral calibration error	1 cm^-1 spectral error and 5K diff. between BB and std T	CAL/IFC	Apply reqmt to s/s
7	Scan Stray: Scan mirr.av.T	Av. temp of beam footprint changes 10mK in el 100mK in Az	TEL	Apply reqmt to s/s
8	Scan Stray: x term	x=1.5e-4, known to 20%	TEL	Apply reqmt to s/s
9	Scan Stray: y and z terms	Initial estimate based on TC-RAL-043B	TEL	More Anal required
10	Scan Stray: x' term	x'=1.e-3, scan mirror T within 4K of IFC BB	TEL	Apply reqmt to s/s
11	Scan Stray: y' and z' terms	Effective coeff=2.e-4 Radiance ratio=0.5	TEL	More Anal required
12	Scan Stray: Diffraction	Initial estimate based on TC-RAL-043B	TEL	More Anal required
13	Uncorrected non-linearity	0.1% slope error	DET/CAL/ SPU	Analysis required
14	Electronic offset change	change over 10 s: NEN/4/sqrt(12)	SPU	Apply reqmt to s/s
15	Synchronous jitter	Jitter = 1 microrad = 3 m.	TEL	Apply reqmt to s/s

3. Notes on Analyses required

3 The IFC BB effective emissivity also controls the IFC paraboloid scatter spec. The RAL stray light model will guide this spec and the derived contamination spec.

9, 11 The RAL stray light model will guide these requirements and the derived contamination spec

12 I'm not sure whether we are expecting improved diffraction numbers as well?

13 Somebody, probably Lockheed, must do an analysis of radiation effects on the analogue (and perhaps digital) electronics to see if this requirement is reasonable, and what level of shielding is implied.

One error source not included here is polarization of the IFC view. Very simple calculations indicate that the effect is orders of magnitude too small to worry about, but a slightly better analysis would be valuable.

Further work on RADMETAC includes taking account of these analyses when available, and further study of the best way to treat the scan stray components of the error budget, which may be significantly overestimated at present.

RADMETAC BUDGET: SLOPE ERRORS (in percent)

Last Changed: 950405

SOURCE	CHANNEL >	1	2	3	4	5	6	7	8	9	10	11	12	13	14	15	16	17	18	19	20	21
IFC BB temperature error		0.07	0.08	0.08	0.08	0.08	0.10	0.10	0.11	0.11	0.12	0.12	0.14	0.15	0.15	0.15	0.15	0.16	0.17	0.17	0.18	0.19
IFC mirror temp. error		0.01	0.01	0.01	0.01	0.01	0.01	0.01	0.01	0.01	0.01	0.01	0.01	0.02	0.02	0.02	0.02	0.02	0.02	0.02	0.02	0.02
IFC BB/mirror temp. diff		0.01	0.01	0.01	0.01	0.01	0.01	0.01	0.02	0.02	0.02	0.02	0.02	0.02	0.02	0.02	0.02	0.02	0.02	0.02	0.03	0.03
Deficit IFC BB emissivity		0.15	0.15	0.15	0.15	0.15	0.15	0.15	0.15	0.15	0.15	0.15	0.15	0.15	0.15	0.15	0.15	0.15	0.15	0.15	0.15	0.15
Radiometric offset change		0.00	0.00	0.00	0.00	0.00	0.00	0.00	0.00	0.00	0.00	0.00	0.01	0.01	0.01	0.01	0.01	0.01	0.01	0.01	0.01	0.01
Gain stability		0.13	0.13	0.13	0.13	0.13	0.13	0.13	0.13	0.13	0.13	0.13	0.13	0.13	0.13	0.13	0.13	0.13	0.13	0.13	0.13	0.13
Spectral calibration error		0.01	0.01	0.01	0.01	0.01	0.01	0.01	0.01	0.01	0.01	0.01	0.01	0.01	0.01	0.01	0.01	0.01	0.01	0.01	0.01	0.01
Scan Stray: Scan mirr.av.T		0.00	0.00	0.00	0.00	0.00	0.00	0.00	0.00	0.00	0.00	0.01	0.01	0.01	0.01	0.01	0.01	0.01	0.01	0.01	0.01	0.01
Scan Stray: x term		0.01	0.01	0.01	0.01	0.01	0.01	0.01	0.01	0.01	0.01	0.01	0.01	0.01	0.01	0.01	0.01	0.01	0.01	0.01	0.01	0.01
Scan Stray: x' term		0.01	0.01	0.01	0.01	0.01	0.01	0.01	0.01	0.01	0.01	0.01	0.01	0.01	0.01	0.01	0.01	0.01	0.01	0.01	0.01	0.01
Scan Stray: y',z' terms		0.01	0.01	0.01	0.01	0.01	0.01	0.01	0.01	0.01	0.01	0.01	0.01	0.01	0.01	0.01	0.01	0.01	0.01	0.01	0.01	0.01
Scan Stray: Diffraction		0.00	0.00	0.00	0.00	0.00	0.00	0.00	0.00	0.00	0.00	0.00	0.00	0.00	0.00	0.00	0.00	0.00	0.00	0.00	0.00	0.00
Uncorrected non-linearity		0.10	0.10	0.10	0.10	0.10	0.10	0.10	0.10	0.10	0.10	0.10	0.10	0.10	0.10	0.10	0.10	0.10	0.10	0.10	0.10	0.10
Electronic offset change		0.01	0.01	0.01	0.01	0.01	0.00	0.00	0.00	0.00	0.00	0.00	0.00	0.00	0.00	0.00	0.00	0.00	0.00	0.01	0.00	0.00
Synchronous jitter		0.06	0.03	0.04	0.05	0.05	0.17	0.14	0.13	0.14	0.08	0.06	0.11	0.15	0.09	0.05	0.04	0.08	0.15	0.18	0.09	0.08
	TOTAL (RMS)	0.25	0.24	0.24	0.24	0.24	0.30	0.28	0.28	0.29	0.27	0.26	0.28	0.31	0.29	0.28	0.28	0.29	0.32	0.34	0.30	0.31
	TOTAL (SUM)	0.60	0.56	0.57	0.58	0.58	0.72	0.70	0.69	0.71	0.66	0.65	0.71	0.77	0.71	0.68	0.67	0.72	0.79	0.84	0.75	0.76
	REQUIREMENT	1.00	0.50	0.50	0.50	0.50	1.00	1.00	1.00	1.00	1.00	1.00	1.00	1.00	1.00	1.00	1.00	1.00	1.00	1.00	1.00	1.00

RADMETAC BUDGET: ZERO ERRORS (in NENs)

Last Changed: 950405

SOURCE	CHANNEL >	1	2	3	4	5	6	7	8	9	10	11	12	13	14	15	16	17	18	19	20	21
Radiometric offset change		0.01	0.02	0.03	0.04	0.04	0.06	0.07	0.16	0.06	0.09	0.10	0.12	0.10	0.14	0.11	0.09	0.16	0.15	0.04	0.24	0.11
Gain stability		0.02	0.02	0.05	0.05	0.05	0.06	0.07	0.16	0.06	0.08	0.09	0.10	0.07	0.10	0.08	0.06	0.10	0.10	0.03	0.14	0.06
Scan Stray: Scan mirr.av.T		0.01	0.01	0.02	0.03	0.03	0.04	0.05	0.11	0.05	0.06	0.07	0.09	0.07	0.10	0.08	0.06	0.11	0.11	0.03	0.17	0.08
Scan Stray: x term		0.10	0.11	0.23	0.26	0.26	0.31	0.34	0.78	0.31	0.40	0.43	0.48	0.35	0.50	0.39	0.30	0.51	0.48	0.13	0.72	0.31
Scan Stray: y and z terms		0.01	0.01	0.01	0.02	0.03	0.11	0.13	0.32	0.13	0.13	0.07	0.25	0.17	0.16	0.07	0.04	0.11	0.12	0.04	0.14	0.07
Scan Stray: Diffraction		0.04	0.03	0.06	0.07	0.08	0.23	0.25	0.58	0.23	0.19	0.10	0.28	0.17	0.15	0.06	0.04	0.09	0.09	0.03	0.09	0.04
Electronic offset change		0.07	0.07	0.07	0.07	0.07	0.07	0.07	0.07	0.07	0.07	0.07	0.07	0.07	0.07	0.07	0.07	0.07	0.07	0.07	0.07	0.07
Synchronous jitter		0.03	0.03	0.04	0.04	0.04	0.06	0.03	0.07	0.04	0.07	0.05	0.05	0.03	0.04	0.04	0.04	0.03	0.02	0.11	0.03	0.02
	TOTAL (RMS)	0.13	0.14	0.26	0.29	0.30	0.42	0.47	1.06	0.42	0.49	0.49	0.64	0.45	0.59	0.44	0.34	0.58	0.55	0.20	0.81	0.37
	TOTAL (SUM)	0.28	0.30	0.52	0.58	0.60	0.95	1.01	2.24	0.95	1.08	1.00	1.43	1.03	1.26	0.91	0.70	1.18	1.14	0.47	1.60	0.77
	REQUIREMENT	1.00	0.50	0.50	0.50	0.50	1.00	1.00	1.00	1.00	1.00	1.00	1.00	1.00	1.00	1.00	1.00	1.00	1.00	1.00	1.00	1.00

The Radiometric Calibration Budget for the High Resolution Dynamics Limb Sounder.

C. W. P. Palmer and J. G. Whitney.

Atmospheric, Oceanic and Planetary Physics,
Oxford University, UK.

Abstract.

HIRDLS is a 21 channel infrared filter radiometer due to be launched on the Earth Observing System Chemistry platform in 2002. The channels range in wavelength from 6.1 to 17.8 μm, with fractional widths of between 1% and 8%. The scientific objectives include the retrieval of atmospheric temperature and distributions of a range of minor constituents, the retrieval of geopotential height gradients and the detection of atmospheric wave activity, by sounding the atmospheric radiance viewed at the Earth's limb. These objectives require extremely accurate radiometry, with stringent limits on both errors that scale with the radiance and systematic offsets. The analysis presented shows explicitly how systematic errors in the in-flight calibration propagate into radiometric errors. Initial budget allocations to these error sources are made. An indirect calibration view of a small black body, rather than a full-aperture calibrator, is shown to have advantages in the case that the black body and the telescope optics are at the same temperature. The origins of scan-dependent offsets are discussed, and shown to be significant error sources unless in-flight correction is possible. Two approaches for this are discussed.

1. Introduction

The High Resolution Dynamics Limb Sounder (HIRDLS) is a 21-channel infra-red limb-scanning filter radiometer to be flown on the NASA Earth Observing System Chemistry (EOS-Chem) satellite, due for launch in 2002. The EOS-Chem payload, as currently planned, consists of HIRDLS, the Microwave Limb Sounder (MLS), a Japanese (NASDA) instrument similar to the Total Ozone Mapping Spectrometer and the Tropospheric Emission Spectrometer (TES). The major measurement objectives of the EOS-Chem platform are global measurements of the processes that control ozone, and the rôle of water vapour, aerosols and ozone in climate change.

HIRDLS is being developed jointly by a US/UK collaboration consisting of the National Center for Atmospheric Research (NCAR) in the US and Oxford University and the Rutherford Appleton Laboratory in the UK, under the direction of the joint principal investigators Dr. J. C. Gille (NCAR) and Dr. J. J. Barnett (Oxford University). The instrument concept (Gille and Barnett 1992) has been derived from the instruments LIMS (Gille and Russell 1984) and SAMS (Drummond *et al.* 1980) on Nimbus-7 and ISAMS (Taylor *et al.* 1993) on UARS, and like them it operates by measuring radiance profiles in several channels in the 15 μm CO_2 band in order to determine temperature profiles, and then using these temperatures in conjunction with radiance profiles in other channels to determine fields of trace gases. The emissions in any spectral channel cannot be assumed to be due to a single species, so that in practice a joint retrieval of several data products simultaneously may be required. In particular, radiances in any channel may be contaminated by aerosol emission, and several channels are included for which aerosol emission dominates to enable its effects to be corrected in the other retrievals. The 21 HIRDLS channels and target species are shown in Table 1.

The science objectives of HIRDLS depend on the high spatial resolution of its observations. Its above-mentioned predecessors viewed the limb at a fixed angle to the direction of flight, so obtaining observations along a single track for each orbit, whereas HIRDLS will view the limb to the rear of the spacecraft, and use cross-track scanning to generate a swath of profiles 2000–3000 km wide. Swaths on adjacent orbits will overlap, giving global coverage every 12 hours with a grid of profiles having a maximum spacing of 4° in latitude and longitude. In addition the vertical resolution, which for a limb sounder is usually determined by the vertical extent of the field of view, has been reduced to 1 km. These resolutions have been chosen to be comparable in a dynamical sense, so that structures in the atmospheric flow are expected to have these relative dimensions in the horizontal and vertical respectively, and consequently these are the proportions usually chosen for grid spacings in numerical models. (Earlier sounders have significantly lower resolution in this sense in either the vertical or horizontal, depending on whether they are nadir- or limb-sounding instruments.)

The high spatial resolution should permit a number of new studies including a better understanding of the spatial distribution of stratosphere-troposphere exchange, observation of larger scale gravity waves and layered structures in the stratosphere, as well as the provision of valuable higher resolution data for the validation of numerical models. Other objectives include obtaining climatologies and trends for a range of data products. A new type of measurement being attempted is the retrieval of geopotential height gradients.

Temperature sounding by limb-scanning instruments has always relied on the fact that over a range of heights in the middle atmosphere the observed radiances allow the retrieval of the pressure at the tangent point (Gille and House 1971); this considerably relaxes the requirements on absolute pointing knowledge for correct location of the radiances. However it also allows the possibility that if precise knowledge of the change in pointing from one profile to the next is available then the geopotential height gradient can be inferred, and HIRDLS will carry its own gyroscope unit mounted on the optical bench for this purpose.

A schematic of the instrument layout is shown in Figure 1. This represents the baseline design, which is still being refined in several areas. A telescope forms an image of the field stop of each channel in the atmosphere at the limb, approximately 10 km $\times$ 1 km high. In the baseline design the field stops are defined by the individual HgCdTe detector elements, which are located in a cooled focal plane array, while the array of filters defining the spectral bandpass is located in an intermediate field image plane. The radiation from the atmosphere is chopped at the primary focus by a rotating toothed mirror chopper with a view to space, and the location of the field in the atmosphere is controlled by a plane scan mirror in front of the primary, which can be scanned in the elevation (height) and azimuth (cross-track scan) directions. The outputs from the detectors are amplified, digitized, synchronously demodulated and digitally filtered. This scheme allows considerable flexibility in programming the rates of scanning, type of digital filtering and selection of channels for measurement and telemetry rate (subject to an overall telemetry bandwidth limit) but the baseline scheme is for all channels to be telemetered every 12 ms, corresponding to 6 chopper cycles, with a scan pattern such that this corresponds to a vertical motion of the field of view (FOV) of 0.2 km. Thus there is significant over-sampling in order to determine uniquely the resolution-limited radiance profile.

The present paper is concerned with the radiometric accuracy of HIRDLS. The In-Flight Calibration (IFC) will be described in detail in section 3 below, but Figures 1 and 2 show the elements of the scheme. The scan pattern will consist of a number, typically 6, of vertical scans at different azimuths in one cross-track scan, and each of these profiles will be extended upwards sufficiently high that the expected atmospheric radiance is zero. Thus a zero reading is taken from this space view every 20 s. As part of the 'flyback' of the scan mirror in order to begin the next azimuth scan a view of a black body at a fixed temperature (approximately 300 K) will be obtained, to give a 'full scale' reading every 66 s. These two views of known radiance, and the assumption that the signal channel transfer characteristic is known, are sufficient for the in-flight calibration. Systematic errors in this scheme will be analysed in sections 3 and 4, and their size estimated in section 5. Other aspects of the instrument calibration also present interesting and difficult measurement problems, in particular the geometrical aspects of the calibration (the motion of the scan mirror and the definition of the FOV). These will only be be referred to briefly in section 3, and the methods to be used will be described in a later publication.

2. Derivation of Radiometric Performance Requirements

The science objectives described above lead to some very stringent performance requirements over the projected 5-year operational lifetime of the HIRDLS instrument in orbit. The nominal orbit for the EOS-Chem platform is 705 km altitude and 98.2°inclination, leading to an estimated total ionizing dose radiation environment of 30 kRad behind 1 mm of Al (perpetual solar maximum estimate). The requirements are set out in the Instrument Requirements Document (IRD, Gille and Barnett 1994), which addresses all aspects of the instrument and pre-flight calibration system requirements. A number of system-level budgets relating to specific IRD requirements have been created, either allocating permissible errors to various sources, or summing different contributions to the same quantity. These include, for example, error budgets for pointing knowledge in elevation and azimuth, and a spectral blocking budget that totals the out-of-band blocking contributed by the various optical components in the system. In this section we shall briefly describe the requirements and controlling budgets for radiometric quantities, discussing first random noise levels, and then the allowable systematic radiometric errors, which form the main topic of the paper.

Specifying the random noise level is complicated by the flexibility described above to change the on-board digital filtering which occurs before transmission to the ground. Thus a search for gravity waves might employ a special digital filter with improved performance at some frequency of interest, and a consequent side-effect on noise bandwidth. The solution adopted in the IRD is to set levels for the Noise-Equivalent Radiance (NEN) in a standard bandwidth of 7.5 Hz. This roughly corresponds to integration for the time taken for the FOV to be scanned by its own height in the baseline scanning pattern. These noise levels are very low, as small as $4 \times 10^{-5} B(300)$ in some channels, where $B(300)$ is the radiance of a 300 K black body. This is a relevant unit, since the signal channel must have sufficient dynamic range for the IFC black body view. However most atmospheric radiances are significantly smaller, so the signal:noise ratio in the atmospheric radiances will not be so large. Potential noise sources include chopping instablility and analogue signal processing (pre-amplifier and digitizer) in addition to intrinsic detector noise. One system-level budget allocates noise to these sources. It is important to keep the noise from such sources strictly under control and to ensure the maximum transmission of the wanted signal through the optical system to the signal processing electronics. For HIRDLS, a detailed throughput budget has been compiled for each of the 21 spectral channels. The transmission factor of each of the many optical surfaces has been estimated, as well as that of the bulk refractive elements such as the common detector Dewar window and the individual bandpass filters. These two budgets permit the specification of the required detectivity for the detectors. (In orbit, an additional source of noise is jitter in the Instantaneous Line Of Sight (ILOS) in the presence of atmospheric radiance gradients. However the IRD NEN requirements are to be met in the absence of this noise source, because jitter is the controlled by other specific IRD requirements.)

The IRD requirement on systematic radiometric error is that it must not exceed the equivalent of 1% of the measured atmospheric radiance, or the specified random noise level, whichever is the larger, with a stated design goal of 0.5% of the radiance or a quarter of the noise level, particularly in Channels 2–5. The design goal has been partially incorporated into the instrument specification by adopting 0.5% or 0.5 NENs as the requirement for the

temperature-sounding channels 2–5, but there remains the stated desire to achieve similar accuracy for all channels. These requirements imply that the end-to-end radiometric zero stability over time periods from 12 milliseconds to 10 seconds must be equivalent to 1 part in 25,000 in at least some channels. This, as we shall see, is an extremely tall order for a thermal radiometer in Low Earth Orbit with a 0.5 square metre viewing aperture and whose scanning mirror operates with angles of incidence which vary significantly within this timescale. As a slight mitigation of this requirement we should note that it refers only to specifically radiometric errors, and not to errors of interpretation due to errors in the knowledge of the FOV, ILOS or spectral bandpass, which are the subject of other IRD requirements, though of course errors from these sources can be expressed as equivalent radiometric errors.

The radiometric systematic accuracy requirement obviously applies at system level, and it is necessary to identify all significant potential sources of error, and then to perform a notional, maximum allocation to each — in other words, to compile a system-level radiometric error or accuracy budget. At least 15 significant sources of systematic radiometric error have so far been identified; these fall into one of the following categories: error in the determination of the IFC 'zero' radiance, error in the determination of the IFC 'full scale' (black body) radiance, error in the pre-launch characterisation of the IFC black body radiance vs. temperature telemetry, error in the knowledge of the non-linearity of the end-to-end signal channel transfer functions, and ILOS jitter synchronous with the chopper.

Having determined a target transmission factor for each radiometric component and an initial and, to some extent arbitrary, allocation of the maximimum allowable error from each systematic error source, it is possible to list the detailed radiometric performance requirements for each instrument subsystem, subassembly or component as appropriate, as well as the performance requirements of the pre-launch ground calibration facility.

3. Calibration of Radiometers.

In this section we shall describe the way the in-flight calibration, combined with the pre-flight characterisation of the instrument, defines the measured radiances. This allows us in section 4 to carry out an error analysis on this procedure, and so determine the components of the error budget.

If we assume that the output count in each channel is a linear function of the photon arrival rate at all points across the detector then the telemetered digital count S is related to the spectral radiance at the entrance pupil N by

$$S = C + G \int F(\mathbf{x}, \mathbf{n}, \bar{\nu})\, N(\mathbf{x}, \mathbf{n}, \bar{\nu})\, d^2\mathbf{x}\, d\Omega\, d\bar{\nu}. \tag{1}$$

In (1):

C is the offset count, defined as the output count with zero radiance at the entrance pupil, which has contributions from electronic offsets and the radiometric offset, which is the radiometric difference between the direct view to space through the telescope and the space reference view in reflection from the chopper;

N is the spectral radiance at the entrance pupil of the radiometer, defined by the vector $\mathbf{x}$ giving the location in the entrance pupil of differential area $d^2\mathbf{x}$, the unit vector $\mathbf{n}$ which defines the direction at the entrance pupil of the differential solid angle $d\Omega$, and the wavenumber $\bar{\nu}$ of the differential band $d\bar{\nu}$;

F is the instrument averaging function, defining the form of the spatial, spectral and angular averages over the spectral radiance incident at the entrance pupil performed by the radiometer, and

G is the system gain, including the reflectivities or transmissions of spectrally flat optical elements, efficiency of the optical chopping/synchronous demodulation signal processing and electronics gain.

Several points about the definition of F in (1) should be made. Since F and G simply multiply each other, we can move constant factors (independent of $\mathbf{x}$, $\mathbf{n}$ and $\bar{\nu}$) between F and G, allowing us to define the normalization of F. We choose to define the integral over F to be unity, in line with its definition as an averaging function:

$$\int F(\mathbf{x}, \mathbf{n}, \bar{\nu})\, d^2\mathbf{x}\, d\Omega\, d\bar{\nu} \;=\; 1.$$

This has the effect that if the radiometer views a (spectrally and spatially) uniform radiance then (1) simplifies to

$$S \;=\; C \;+\; G\,N$$

so that the gain factor G also contains the étendue ($A\Omega$) and spectral bandwidth factors for the channel. Secondly, if $\mathbf{l}$ is a unit vector normal to the entrance pupil plane then the power crossing area $d^2\mathbf{x}$ contained in the solid angle $d\Omega$ and spectral interval $d\bar{\nu}$ is $N(\mathbf{x}, \mathbf{n}, \bar{\nu})\, \mathbf{n} \cdot \mathbf{l}\, d^2\mathbf{x}\, d\Omega\, d\bar{\nu}$; the $\mathbf{n} \cdot \mathbf{l}$ factor, which is the cosine of the angle between $\mathbf{n}$ and $\mathbf{l}$, is in principle contained in F. Finally, the detectors used in HIRDLS are (as implied above) photon detectors and not bolometers, and the photon flux is related to the energy flux by a factor of $hc\bar{\nu}$; the variation of this factor over the spectral interval covered by the channel is also in principle included in F.

Equation (1) looks like a very general model of a radiometer, but it depends on two linearity assumptions that can be criticized: overall linearity (doubling all radiances doubles the contribution to S) and spatial additivity (the effects of radiance incident on different parts of the detector just add). Overall linearity is an important property of the radiometer, since it allows us to extract the filtered radiance from a two-point in-flight calibration scheme. Both the detector itself, and the following electronics, are possible sources of non-linearity. Spatial additivity, on the other hand, is a property required of the detector. It appears to be a plausible assumption provided the chopped signal is a small perturbation on the unchopped background of photons incident on the detector. In the case of HIRDLS, the background:signal ratio is only about five in many channels, when viewing the IFC black body, so that this condition is not obviously satisfied. The assumption of spatial additivity would not matter if the incident radiance were always close to uniform across the detector. However, the pre-launch mapping of the FOV is carried out by scanning a small hot source over the field, so that in the baseline design, where the field stop is formed by the detector, this generates very non-uniform illumination of the detector. This assumption will therefore need to be examined in more detail.

A simplification has also been made in (1) in that it ignores polarization effects. To include them, (1) would have to be generalized to give the radiometer response in terms of all four Stokes parameters of the incident radiation (see, for example, Born and Wolf 1980). It is not expected that under normal conditions the incident radiance will be significantly polarized, so that in orbit it is the polarization-average function F that is relevant. There is then a significant issue relating to the pre-flight measurement of F; since the instrument is not required to be polarization-insensitive, there will inevitably be some polarization sensitivity. The corollary of this is that measurements involving polarized test radiances (such as the output from a grating monochromator) will have to be designed to yield the polarization-averaged F as required. We shall not discuss this further here, because it relates more to the measurement of F than the radiometric calibration.

A final complication to equation (1) is that the function F may have a non-trivial dependence on variable instrument parameters. One obvious example is the dependence of the FOV on the scan mirror position, which in the case of HIRDLS is complicated by the fact that while the FOV always has the same shape (because the scan mirror is plane) it does not always have the same orientation with respect to the vertical direction in the atmosphere. However there may well be more subtle dependences — for example the effective spectral passband may change with instrument temperatures, either as a result of the actual shift of the filter bandpass, or as a result of a change in the spectral variation of detector responsivity with temperature. Another example of a change in F as a result of a change in instrument parameters is a change in the weighting given to different parts of the FOV resulting from changes in the phasing of the demodulation relative to the chopping motion. In summary then, the function F is the goal of pre-launch characterisation,but it represents a vast amount of information, and some simplification or parameterization of its structure is likely to be necessary.

The first simplification is that *in orbit* the radiances at the entrance pupil are undoubtedly uniform across the pupil, since the earth is at such a great distance. Thus in (1) we can suppress the $\mathbf{x}$ argument of N, and carry out the integral over $\mathbf{x}$, defining the optics transmission function averaged over the entrance pupil to be $\bar{F}$:

$$\bar{F}(\mathbf{n}, \bar{\nu}) = \int F(\mathbf{n}, \mathbf{x}, \bar{\nu})\, d^2\mathbf{x} \tag{2}$$

so that (1) becomes:

$$S = C + G \int \bar{F}(\mathbf{n}, \bar{\nu})\, N(\mathbf{n}, \bar{\nu})\, d\Omega\, d\bar{\nu}. \tag{3}$$

The implication of (2) and (3) is not that the optics transmission function F is independent of $\mathbf{x}$ but that, as in the case of polarization, it is only the averaged function $\bar{F}$ that is required to interpret the filtered radiances, because the radiance is independent of $\mathbf{x}$. Since F will in fact depend on $\mathbf{x}$, the corollary of this is that test radiance fields should be uniform over the entrance aperture.

A further simplification is almost invariably made, namely that $\bar{F}$ factorizes:

$$\bar{F}(\mathbf{n}, \bar{\nu}) \;=\; F_{\mathrm{FOV}}(\mathbf{n})\; F_{\mathrm{spec}}(\bar{\nu}) \tag{4}$$

where F_{FOV} and F_{spec} are separately normalised to unity. This approximation allows separate measurement of the FOV function F_{FOV} and the spectral bandpass F_{spec} with a collimator and a monochromator respectively. However it is not difficult to think of effects which will cause it to be invalid; we shall give three examples. Rays from different field positions will always pass through the bandpass filter in slightly different ways; in the baseline design, the bandpass-defining filters are located in a field image plane, so that such rays pass through different parts of the filter, but in another optical arrangement they might pass through at different angles. Thus in the baseline case, spatial non-uniformity of the filter would lead to a breakdown of (4). Secondly the detector responsivity is likely to be non-uniform, and this is likely to correlate with different spectral dependences of the responsivity. The slope of the responsivity across the passband is one of the spectral dependences that determines its shape. Finally, any stray light paths that end on detectors usually have different spectral dependence, because they have been reflected instead of transmitted at one or more optical surfaces, and they typically originate from different field positions from the wanted rays.

The approach which we shall take with HIRDLS is to control effects which lead to a breakdown of (4) to the greatest extent possible, and base our pre-launch characterisation on this approximation, while also attempting to verify it as well as possible. Thus the detector will be required to have a spectrally flat responsivity around the passband which has the dual advantage of reducing both the spectral effect of spatial inhomogeneity, and also the spectral effect of temperature changes. Stray light is thoroughly undesirable for many reasons, and one control to be used is a second set of filters, located directly in front of the detectors. (These have wider passbands than the bandpass-defining filters in the intermediate field image plane, and also have the important function of greatly reducing the background photon flux on to the detector.) Stray light paths passing through one filter in the intermediate plane, and ultimate detection by a *different* detector are thus inhibited by the lack of spectral overlap between the two filters. Careful attention is also being paid to stray light paths in the detailed optical design, ensuring that all sequences of stray reflections lead to a very defocussed low-intensity distribution across the focal plane, and that the anti-reflection coatings are properly specified. When it comes to measuring the spectral bandpass profile F_{spec} we hope to make our main measurements at high resolution with the entrance pupil and the main part of the FOV filled with the monochromator beam, but also make measurements at lower spectral resolution with fractions, perhaps quarters, of the field illuminated in turn, in order to verify the approximation (4).

Assuming, therefore, that the function $\bar{F}(\mathbf{n}, \bar{\nu})$ has been adequately characterised, we can now analyse the intended operation of the in-flight calibration. We shall assume that the IFC space view has zero input radiance, and generates a count

$$S_0 = C \tag{5}$$

and that the IFC black body view is equivalent to a view with the input radiance equal to the Planck function at temperature T_c:

$$S_c = C + G \int \bar{F}(\mathbf{n}, \bar{\nu})\, B(\bar{\nu}, T_c)\, d\Omega\, d\bar{\nu}.$$

Introducing the approximation (4) this simplifies to

$$S_c = C + G \int \bar{F}_{\text{spec}}(\bar{\nu})\, B(\bar{\nu}, T_c)\, d\bar{\nu}. \tag{6}$$

Given a signal count S corresponding to an atmospheric view according to (3), and the counts for the IFC views (5) and (6) we form the calibration ratio $\mathcal{R}$:

$$\mathcal{R} = \frac{S - S_0}{S_c - S_0} = \frac{\int \bar{F}(\mathbf{n}, \bar{\nu})\, N(\mathbf{n}, \bar{\nu})\, d\Omega\, d\bar{\nu}}{\int F_{\text{spec}}(\bar{\nu})\, B(\bar{\nu}, T_c)\, d\bar{\nu}} \tag{7}$$

Equation (7) gives the radiance, averaged over the FOV and the spectral bandpass, in terms of a filtered black body radiance at temperature T_c. Radiances averaged over the spectral profile F_{spec} and, where relevant, the FOV will be denoted by an overbar. Equation (7) then reads $\bar{N} = \mathcal{R}\bar{B}(T_c)$. For the purposes of comparing this to a forward model radiance it is convenient to have it in units of a standard temperature black body radiance at T_0. Thus our final calibrated radiance is

$$\frac{\bar{N}}{\bar{B}(T_0)} = \mathcal{R}\, \frac{\bar{B}(T_c)}{\bar{B}(T_0)} \tag{8}$$

in units of a T_0 black body filtered radiance. (The standard temperature T_0 will be chosen to be very close to the operating point of the IFC black body, so this factor will be very close to unity.)

Radiometers of this type are sometimes referred to as self-calibrating, which is a misnomer because they do still require extensive calibration and characterisation before use, in order to determine their averaging function $\bar{F}$. Their special property is that the extraction of the measured radiance, as in (8), does not depend crucially on $\bar{F}$. (We shall find in section 5 that the effect of the dependence on F_{spec} is very small.) The importance of an accurate knowledge of $\bar{F}$ is for the correct interpretation of the measured radiance, so that the requirements on such knowledge derive not from the radiometric requirements but from other considerations. We shall not therefore discuss the measurement of $\bar{F}$ any further here.

Straightforward error analysis on (8) would suggest that if the errors in $\mathcal{R}$ are random, then the systematic errors (that is, correlated over many 12 ms samples) are confined to the knowledge of the effective IFC black body temperature T_c, and the knowledge of the spectral function F_{spec}, for the evaluation of the ratio of filtered Planck functions. Both of these errors scale with the radiance — we shall refer to them as slope errors — and the requirement is that slope errors must be less than 1%. With these two contributions this is a relatively easy requirement to meet, which suggests that 1% radiometry is possible down to the smallest radiances. Unfortunately this is too straightforward an error analysis, which omits a class of errors which are independent of the radiance. These are quite unimportant at large radiance, but dominate at small radiances, and we shall refer to them as zero errors. In order to track these down we must examine the calibration process in more detail.

4. Systematic Errors in Radiometric Calibration

The elementary error analysis in section 3 needs to be extended in three separate areas. First the view presented at the entrance pupil by the IFC black body subsytem needs to be analysed in more detail to determine on what the effective temperature T_c depends. Second, various forms of instrumental instability lead to slope and zero errors, and most of these are covered by a simple analysis. However, in the case of processes ocurring at the scan mirror (reflection and scattering) there are radiometric connections between the resulting slope and zero errors, so these require a third analysis. All of these analyses lead to corrections to the simple calibration algorithm (8).

We first examine the IFC black body view. This is not a view of a full-aperture black body, but of a small black body imaged by an off-axis paraboloid to fill the instrument aperture. The reason for adopting this approach is that a full-aperture target cannot, for space and mass reasons, have the ideal cavity geometry, and would have to be a large, plane structured surface, located near the exterior aperture, and therefore relatively exposed to the space environment. A small cavity-type target can be much blacker, have much better thermal uniformity and be much better protected over the five-year mission than a full-aperture target; the cost of these gains is the indirect view. The IFC paraboloid mirror must therefore be considered as part of the same radiometric system. From this point of view it is a much more desirable full-aperture surface, because the scattering at a high quality optical surface will be much lower than at a surface which is appreciably black at 17 μm. The output filtered radiance from this radiometric system will consist of radiation emitted by the black body (emissivity e_b, temperature T_b), radiation from inside the enclosure N_e reflected from the black body, and radiation emitted by the IFC paraboloid (emissivity $e_{\rm par}$, temperature $T_{\rm par}$):

$$\bar{B}(T_c) = e_b(1-e_{\rm par})\bar{B}(T_b) + (1-e_b)(1-e_{\rm par})\bar{N}_e + e_{\rm par}\bar{B}(T_{\rm par}). \qquad (9)$$

In (9) the reflectivities are assumed to be given by (1 − emissivity). We are thus ignoring scattered radiation, which would generate another term depending on the radiation in the enclosure N_e. The important feature of (9), which would also be true of a more detailed radiometric model, is that it is radiometrically complete, in that the coefficients of the three radiances add up to unity. This implies that if all the radiances are equivalent to the Planck function at the same temperature, then so is the resulting radiance, which is of course a thermodynamically required constraint on the model. Thus the omission of scattering does not really affect the validity of the model provided it is recognized that the model parameters are to a small extent 'effective' parameters: the model value of e_b may embody small corrections resulting from scattering, including scattering at the IFC paraboloid.

This 'completeness' allows (9) to be re-written as the Planck function of the black body plus corrections involving the radiance differences:

$$\bar{B}(T_c) = B(T_b) + e_{\rm par}\left(\bar{B}(T_{\rm par}) - \bar{B}(T_b)\right) + (1-e_b)(1-e_{\rm par})\left(\bar{N}_e - \bar{B}(T_b)\right). \qquad (10)$$

The implication of this is that the combined system provides a perfect calibration radiance to the extent that the whole sub-assembly is enclosed and isothermal. It is envisaged that

the IFC paraboloid and the black body temperatures will be separately controlled, and will be maintained at the same value. Small variations in temperature between them will be allowed for in the calibration algorithm using a measured value of the coefficient $e_{\rm par}$. This can be measured as part of the pre-launch calibration, and periodically re-measured in flight by changing one of the controlled temperatures. Thus the systematic errors in $\bar{B}(T_c)$ are errors in the knowledge of T_b, $T_{\rm par} - T_b$ and $e_{\rm par}$, and the whole of the final term in (10), which is controlled by making e_b as close to unity as possible, and making the radiative environment within the IFC subsystem as isothermal as possible through baffling. These errors are in addition to the spectral error in $\bar{B}(T_c)/\bar{B}(T_0)$ referred to in section 3.

The second extension to the analysis of section 3 is allowance for instrumental instability, leading to slope and zero errors. The key to understanding the origin of these errors is the recognition that in the calibration ratio $\mathcal{R}$ the three signal counts that enter are all measured at different times, and with different orientations of the scan mirror. Time-dependent variations in gain or offset, and processes that lead to changes with scan mirror position, all lead to errors in the differences in $\mathcal{R}$. An error in the denominator leads to a slope error, but errors in the numerator lead to zero errors. We can re-write equations (3), (5) and (6) for the counts in the three views allowing for changes in gain and offset:

$$\begin{aligned} \text{atmospheric view:} \quad & S = C + G\,\bar{N} \\ \text{IFC space view:} \quad & S_0 = C_0 \\ \text{IFC BB view:} \quad & S_c = C_c + G_c\,\bar{B}(T_c) \end{aligned} \tag{11}$$

where the subscripts 0 and c again denote the space and black body views. Forming the calibration ratio we obtain

$$\bar{N} = \mathcal{R}\bar{B}(T_c') - \frac{C - C_0}{G} \tag{12}$$

where

$$\frac{\bar{B}(T_c')}{\bar{B}(T_c))} = 1 + \frac{G_c - G}{G} + \frac{C_c - C_0}{G\bar{B}(T_c)} \tag{13}$$

showing explicitly the zero errors in (12) and the fractional slope errors in (13).

The zero errors in (12) are given by the radiance equivalent to the change in offset count between the atmospheric view and the IFC space view, over a time period of up to 10 s, and an elevation angle change of up to 0.05 rad. Contributions of this sort we might categorize as radiometric and electronic. The radiometric contributions to these offset changes come from temperature changes of the chopper or optics in front of it (scan mirror, telescope primary and relay mirror for the chopper space view). In addition, since the radiometric offset goes through the signal processing chain, changes in overall gain, as discussed below, also produce zero errors. These stability requirements constitute a strong argument for a small value for the radiometric contribution to C_0. Electronic contributions include changes in any electronics offset, and the variable component of any optical or electronic pickup or cross-talk between channels.

The slope errors in (13) are given by the fractional changes of gain between the IFC space and black body views, and zero-type errors between these two views expressed as a

fraction of the black body radiance. Thus all the mechanisms mentioned above for zero errors also produce slope errors, but these are in all cases extremely small, even though the time period involved is longer (66s). In addition, gain instability produces slope errors, and specific mechanisms by which this can occur are a change in the chopping efficiency resulting from a change in chopper motion, a change in the detector responsivity (probably linked to a change in focal plane temperature), and changes in electronics gain (again, probably driven by temperature changes).

We can use the general analysis of (11) – (13) for all the types of instrumental instability discussed above, but not for the important case of changes in the radiative properties of the scan mirror, because the resulting changes in C and G are radiometrically linked. We shall therefore develop a more detailed analysis for the scan mirror, assuming that other aspects of the radiometer are stable (including the scan mirrror temperature, because we have already included the error from that source above).

We need to consider three processes occurring at the scan mirror: the reflection of the input radiance, the thermal emission of the mirror surface (temperature T_s), and scattering of radiation into the radiometer beam. A full definition of these processes would involve complicated integrals over the directional emissivity and the Bi-directional Reflectance Distribution Function (BRDF) of the mirror surface, and the spatial and angular distribution of input radiation outside the wanted beam. Since none of these quantities are or could be known over the whole lifetime of the instrument we shall present a parameterised analysis that contains the necessary radiometric relationship between these three processes. We therefore consider the transformation of the input radiance at the scan mirror to produce the following emitted radiances in the three views:

$$\begin{aligned} \text{atmospheric view:} \quad & R\bar{N}+e\bar{B}(T_s) + \Delta e\bar{N}_e \\ \text{IFC space view:} \quad & e_0\bar{B}(T_s) + \Delta e_0\bar{N}_{e0} \\ \text{IFC BB view:} \quad & R_c\bar{B}(T_c)+e_c\bar{B}(T_s) + \Delta e_c\bar{N}_{ec}. \end{aligned} \tag{14}$$

In (14):

(i) the scan mirror has reflectivity R and emissivity e, which vary with mirror position as indicated by the subscript 0 or c as above;

(ii) the reflectivity is *not* assumed to be (1 − emissivity), but there is an extra term Δe involving radiation inside the optics enclosure N_e scattered into the beam, where radiometric completeness requires $R + e + \Delta e = 1$.

If we now use this relationship to eliminate the emissivities in (14) we can re-write the radiances as:

$$\begin{aligned} \text{atmospheric view:} \quad & R\bar{N}+(1-R)\bar{B}(T_s) + \Delta e\left(\bar{N}_e - \bar{B}(T_s)\right) \\ \text{IFC space view:} \quad & (1-R_0)\bar{B}(T_s) + \Delta e_0\left(\bar{N}_{e0} - \bar{B}(T_s)\right) \\ \text{IFC BB view:} \quad & R_c\bar{B}(T_c)+(1-R_c)\bar{B}(T_s) + \Delta e_c\left(\bar{N}_{ec} - \bar{B}(T_s)\right). \end{aligned} \tag{15}$$

In terms of the previous formalism, the scan mirror reflectivity R in the first terms of (15) is part of the system gain G, and the second and third terms are radiometric offsets that generate part of the offset count C. The radiances in (15) thus contain view-dependent

gains and offsets just like the signal counts in (11), and the remaining parts of the gain and offset which turn these radiances into counts are, for the purposes of this analysis, constant. Thus the whole of (15) is analagous to (11) except for the radiometric linkage between the coefficients, represented by the appearance of the 'gain' R in the emission offset terms. When we form the calibration ratio, we therefore obtain zero and slope errors as in (12) and (13):

$$\bar{N} = \mathcal{R}\bar{B}(T_c') + x\bar{B}(T_s) - y\left(\bar{N}_{e0} - \bar{B}(T_s)\right) - z\left(\bar{N}_e - \bar{N}_{e0}\right) \tag{16}$$

$$\frac{\bar{B}(T_c')}{\bar{B}(T_c)} = (1-x) - x'\frac{\bar{B}(T_s) - \bar{B}(T_c)}{\bar{B}(T_c)} - y'\frac{\bar{B}(T_s) - \bar{N}_{e0}}{\bar{B}(T_c)} - z'\frac{\bar{N}_{ec} - \bar{N}_{e0}}{\bar{B}(T_c)} \tag{17}$$

where in (16) and (17)

$$x = \frac{R - R_0}{R} \qquad x' = \frac{R_c - R_0}{R}$$
$$y = \frac{\Delta e - \Delta e_0}{R} \qquad y' = \frac{\Delta e_c - \Delta e_0}{R}$$
$$z = \frac{\Delta e}{R} \qquad z' = \frac{\Delta e_c}{R}.$$

The zero errors in (16) derive from the change in scan mirror emission at constant scattering (x term) and the change in scattering. The difference between the scattering terms in (15) has been expanded into two terms (the y and z terms) in order to parameterise separately the effects of changes in the scattering power of the mirror between the two views (y term), and changes in the incident radiation field between the two views (z term). This has been done in order to make explicit the two separate error sources that are potentially present here, since the errors are controlled by quite different means — uniformity of the incident radiation by baffling and thermal uniformity, and scattering by BRDF specification and contamination control.

The slope errors in (17) derive from both gain (reflectivity) and offset errors in (15), in the same way as the two slope error terms in (13). The reflectivity change gives rise to a slope error $(R_c - R)/R$, which can be written as $x' - x$ in terms of the defined coefficients. The double appearance of R in both gain and offset terms referred to above now leads to a substantial cancellation, as the slope error resulting from the change in the emission terms in (15) is $-x'(\bar{B}(T_s))/\bar{B}(T_c))$. Since the scan mirror will have a very similar temperature to the IFC black body, this slope error substantially cancels the x' term from the reflectivity change, and since $x' \gg x$ this cancellation is significant for the gain error budget. In physical terms this means that the significant change in scan mirror orientation required to view the IFC BB and hence measure the gain results in changes in both gain and offset which tend to cancel, for the same radiometric reason that the combination of IFC mirror and IFC BB need not be significantly less black than the IFC BB on its own, as discussed above. The remaining scattering terms generate another slope error in (17), which has been split into two terms, the y' and z' terms, just like the zero errors in (16).

This completes our formal analysis of the operation of the radiometer. The result for the desired atmospheric view radiance in terms of a filtered Planck function radiance is

(12), which defines it in terms of the calibration ratio of counts $\mathcal{R}$ defined in (7). A very small correction to a standard temperature Planck function will also be made, as in (8). Zero errors include the various changes with time or scan mirror position discussed above. The calibration Planck function is basically given by (10), with slope errors due to changes with time or scan mirror position as given by (13). As we discussed at the beginning of section (3), all of this analysis is based on a linear response, so that non-linearity is also a source of radiometric error. In practice some of these errors can be reduced to error in the knowledge of the corresponding correction.

5. Radiometric Error Budget and Discussion

The requirements discussed in section 2, and the error sources discussed in sections 3 and 4, suggest the use of separate error budgets for zero and slope errors. In this section we make an initial allocation to these error sources, using a combination of calculation, previous experience and informed estimates, with the aim of setting tight but achievable targets. Many of the individual items in the budget will become the bottom line of their own error budgets; in particular the items relating to the IFC black body and the overall gain will be the resultant of many separate error sources. It is not our intention to allocate the whole of the maximum permitted error, because of the tighter requirements given in the IRD as design goals. Thus this budget is an investigation of the limits to calibration on a 'best efforts' basis within the current conceptual design, and as such it is bound to evolve as the instrument design is finalised.

The budgets are shown in Table 2. All the error sources are channel-dependent, although the actual channel dependence is not known in some cases; the entries in Table 2 are for the worst case channels. The zero errors are given as a fraction of the radiometric noise specified in the NEN column of Table 1, and the slope errors as fractions of a percent, so that the requirements on the totals are that they should be less than 1. Entries left blank are strictly zero according to this analysis, while entries of zero are negligibly small. We shall discuss the entries in turn.

The easiest error sources to estimate are the calculable ones relating to temperature or thermometry. Thus error in knowledge of the IFC black body temperature T_b leads to a slope error of

$$\left(\frac{1}{\bar{B}(T_b)}\frac{\partial \bar{B}(T_b)}{\partial T_b}\right)\Delta T. \tag{18}$$

The bracketed factor is a decreasing function of wavelength, and is thus worst in Channel 21, where it has the value 2.8% K^{-1}. (The temperatures of the IFC and telescope foreoptics are taken to be either 300 K or 290 K, depending on which gives the larger error estimate. In this case it is 290 K.) The table entry is based on an allowable temperature error of 70 mK, to include initial calibration (probably about 35 mK), change after calibration, difference between the radiating surface temperature and the sensor temperature and non-uniformity of the temperature of the black body cavity leading to a different effective temperature. Some of these effects will be measured, or have limits placed on them in the course of pre-launch calibration. Errors in the knowledge of the temperature difference between the IFC paraboloid and the IFC black body lead to a slope error with the same wavelength dependence as (18) but multiplied by e_{par} (see (10)). The table entry is based

on an e_{par} of 0.03 and a temperature error of 0.25 K. This correction also gives rise to an error (with the same channel dependence) if the value used for e_{par} is in error; the table entry is based on an error of 0.01 and a temperature difference of 1K. The remaining error source in (10) is the final term, which cannot be corrected for because of its dependence on stray radiation. The table entry is based on a black body 'effective' emissivity e_b (*cf.* the discussion in section 4) of 0.997 and an input radiance differing from the Planck radiance by 50%, giving a channel-independent error of 0.15%.

A different channel dependence is predicted for the zero errors arising from temperature changes in the telescope foreoptics between atmospheric and space views. There will be an orbital period temperature cycle of many instrument temperatures, driven by the variation in thermal input as the satellite goes in and out of sunlight, and there may be a tendency for peak rates of change to be concentrated around sunrise or sunset, and thus correlated between different parts of the instrument. There are four mirror surfaces contributing to the radiometric offset in the telescope, the scan mirror and the telescope primary in the atmospheric view, and the mirror chopper and a relay mirror in the space reference view. The offset is given by the difference in emission between these two views. In view of the likely correlation between mirror temperatures the table entry is based on the pessimistic assumption that the contributions in each view will be correlated and so add linearly, whereas the two views are uncorrelated, so that the changes do not cancel but add in quadrature. The radiometric offset contributed by, for example, the scan mirror is $e_s \bar{B}(T_s)$, so the zero error in NENs is given by

$$e_s \left(\frac{1}{\mathrm{NEN}} \frac{\partial \bar{B}(T_s)}{\partial T_s} \right) \Delta T_s \tag{19}$$

The bracketed factor is largest in Channel 20, where it has the value 570 K^{-1} (at 300 K). The table entry is based on an emissivity of 0.03 and a temperature stability of 5 mK over 10 s, giving a zero error of 0.09 NENs, multiplied by $2\sqrt{2}$ for the four surfaces. The slope error corresponding to this zero error (as given by the last term of (13)) has the wavelength dependence of (18). The time period over which this instability operates is longer than for the zero error, but like the IFC paraboloid temperature error its effect is reduced by the mirror emissivity, and the slope error is almost negligible.

A related thermal error is generated by the beam shift on the scan mirror in the presence of a temperature distribution over the reflecting surface. The elevation rotation axis is required to be within 1 mm of the scan mirror surface in order to minimise the beam shift, so that a linear temperature variation of 1 K across the mirror produces a very small change in the effective value of T_s of less than 1 mK. Quadratic temperature variation is also likely (for example the centre of the mirror may be colder than the edge), and this also generates a change in the effective value of T_s with elevation scan, as the beam will change its shape on the scan mirror. A simple calculation of the change in the effective value of T_s over the elevation scan range shows that the effect is largest at large azimuth. The table entry is for a 1 K temperature difference between the centre and edge of the scan mirror, which produces a ΔT_s of 10 mK in an elevation scan, and a worse case of 100 mK between the IFC BB view and the space view.

These contributions to the radiometric offset will be multiplied by the overall gain, so there is also a zero error due to gain changes over a 10 s period, while gain changes

over 66 s will lead to slope errors. The table entry is based on a gain change of 2×10^{-5} per second, giving rise to a slope error of 0.13%. To estimate the zero error we require the total size of the radiometric offset. The table entry is based on 0.03 of a 300 K black radiance. This is the offset from one telescope mirror in the above allocations, which is a good estimate for the radiometric imbalance between the two views. This entry includes all sources of gain change other than the scan mirror properties, which we consider below.

The final error source for which we can make elementary calculations of channel dependence is error in the correction of radiances to a standard black body temperature, the final factor in (8). If T_c and T_0 differ by ΔT, and the filter used to calculate the filtered Planck functions is in error by a shift of $\Delta\bar{\nu}$, there will be a slope error of

$$\left(\frac{\partial}{\partial\bar{\nu}}\left(\frac{1}{\bar{B}(T)}\frac{\partial\bar{B}(T)}{\partial T}\right)\right)\Delta T\Delta\bar{\nu}.$$

The bracketed factor is largest for Channel 3, where it has the value 1.7×10^{-7} $\mathrm{m^{-1}K^{-1}}$. Thus even a large temperature correction such as 5 K, and a large filter error such as 1 $\mathrm{cm^{-1}}$(much larger than is permissible for spectral reasons) only lead to the very small slope error in the table entry. Note that this error is the radiometric difference between the radiance actually detected and our calibrated value. There is a much larger difference between the radiance actually detected and that which would have been detected had the filter not been in error, but this is covered by a different system-level error budget, as explained in Section 2.

The most serious zero error is almost certainly the x term in (16), which is the effect of change in scan mirror reflectivity between the atmospheric and space views. This is because x multiplies the Planck function of the scan mirror, whereas the other error terms in (16) multiply relatively small radiance differences. The zero error in NENs has the form

$$\left(\frac{\bar{B}(T_s)}{\mathrm{NEN}}\right)x. \tag{20}$$

The bracketed factor is largest in Channel 8, where it has the value 2.6×10^4, but x will probably have a channel dependence as well. A number of different processes could generate contributions to x: the most obvious is that the reflectivity of the clean mirror surface will vary with angle, but also the reflectivity deficit due to scattering will vary with angle, and the area of mirror surface over which the reflectivity must be averaged to obtain the effective value will vary with scan angle, so that any non-uniformity will affect the averaged value differently at different angles. To set a lower limit on x we consider the variation of the polarization-averaged reflectivity with angle for a good reflector described by a complex refractive index. In the limit of both real and imaginary parts being much greater than one (a good approximation for metal surfaces in the mid-infrared) there is a simple expression for the reflectivity R as a function of the angle of incidence θ (for θ not too close to grazing incidence; see, for example, Stratton 1941):

$$R(\theta) \approx 1 - \left(\frac{1-R(0)}{2}\right)(\cos\theta + \sec\theta) \tag{21}$$

which relates the angle-dependence to the normal reflectivity. The angle of incidence varies with both azimuth and elevation, being centred around 25° at zero azimuth and 33° at maximum azimuth for atmospheric views. It is the latter case that generates the larger value of x, which turns out to be on the order of $0.0025(1 - R(0))$ over the whole elevation scan range at maximum azimuth, or about 7.5×10^{-5} for a mirror with a reflectivity of 0.97. According to (20) this will then generate a zero error of 2.0 NENs in Ch 8, larger than the maximum permitted zero error from all sources. This calculation is undoubtedly pessimistic in some ways: the scan range has been taken to be the whole atmospheric range, whereas the zero errors become negligible compared to slope errors after a fraction (about a quarter) of the scan range, and robust mirror surfaces (such as overcoated gold) are available with a reflectivity more like 0.98 than 0.97. On the other hand this is the irreducible intrinsic effect; surface roughness, contamination and non-uniformity can only make it worse. We therefore use 1.5×10^{-4} as a very rough estimate for the value of x, recognizing that it will have to be much better characterised at a later stage. It is therefore necessary to make some correction to the measured radiances to subtract out this source of zero error, which corresponds to about 4 NENs in Channel 8 over the full scan range.

This is the largest of a group of errors which cause the radiometric offset to vary systematically with scan angle, an effect which we term *scan stray*. Other errors of this type are the effect of scan mirror thermal gradients discussed above, and the y and z terms discussed below. Uncorrected scan stray represents the most serious problem for high-accuracy measurement of small radiances with a HIRDLS-type radiometer. Fortunately to a large extent the scan stray can be corrected; in fact two defences are available to us. Firstly, every elevation scan is extended sufficiently high that space is viewed over a range of angles, to enable not only the offset but also its variation with angle to be determined. The scan stray is expected to be a smooth function of mirror position, so that this observed variation can be extrapolated to at least the upper part of the atmospheric scan, in which the zero errors dominate the slope errors (radiances $\lesssim 100$ NENs). Secondly, the scan stray can be measured directly in orbit, by pitching the spacecraft slightly so that over the whole of the normal scan range there is zero space view at the entrance pupil. This operation is to be repeated at intervals of about three months during the mission. The pitch-up manoeuvre induces a thermal perturbation, and also removes some of the sources of scattered radiation, so that some components of the measured scan stray will not be equivalent to the operational scan stray; however the x component should be identical. It is envisaged that HIRDLS will be scanning throughout the manoeuvre, and some components of the measured stray can be correlated with measured mirror temperatures and emissivities to interpret the data. Detailed planning of this is not at an advanced stage, but the calibration algorithm will use some optimal combination of extrapolated and measured scan stray to correct the radiances.

The allowances for systematic error in the budget have therefore to include the error in the measurement of x, or the change in its value since it was measured, and the error in the cancellation of the y and z terms due to the unrepresentative thermal and radiative conditions during the scan stray measurement. The table entries here are very uncertain: the x allowance is based on a 20% error in x of the order of 1.5×10^{-4}. This term also leads to a slope error, because of the presence of x in (17); the table entry is based on a larger

error in x, because the value used will be corrupted by the y and z terms as mentioned above but even so the slope error is very small. Stray light modelling of the telescope is currently in progress, but a simplified estimate of the y and z terms is already available (Richards,1995), based on an assumed scan mirror BRDF. The estimated value of x' is of order 10^{-3}, but the slope error is significantly reduced by the assumption that the scan mirror will be within ± 4 K of the IFC BB temperature, as emphasized above. y' and z' are estimated to be significantly smaller than x' (Richards 1995), so that even with larger radiance differences the slope error is still very small.

There is a question of definition for the z scattering term associated with the change in radiation scattering into the beam at the scan mirror. It is implicit in sections 3 and 4 that the detected radiation labelled $\bar{N}_e$ has originated from within the instrument, since radiation from the external scene appears in the integral over the instrument averaging function $\bar{F}$, as in (3). In practice there are limits to how large a field can be mapped, and the size of signal that can be distinguished from zero. There will be a field mask at the primary focus defining the composite field of all channels; the individual channel field stops are located further back in the telescope. The FOV function of each channel will be mapped over the whole of this composite field mask, with some border around it. Radiation from outside this region scattered into the beam (earthshine, reflected solar radiation) is then a source of error, and is to be included in the z term. This is, of course, precisely the radiation which leads to scan stray which is *not* corrected by our scan stray measurement, because the pitch-up which takes the atmosphere away from the field of view takes away the error source as well, so it is important to define where in the error budget this is allocated, and also to undertake a proper stray light analysis to support the allocation. Another error source of the same sort is diffraction of bright radiation at the entrance aperture, for which there is a separate entry, also derived from Richards (1995).

The allocation to uncorrected non-linearity is fairly arbitrary, pending a more detailed analysis of the effects of ionizing radiation on the signal channel electronics, but provided the circuits are well-designed the allocation is believed to be on the right order of magnitude. In our discussion of offset changes above we treated only the radiometric offset; there will also be an electronic offset which is required to be stable; the table entry is based on a radiance-equivalent offset change over 10 s of $\mathrm{NEN}/(4\sqrt{12})$, which is in line with the corresponding allocation in the noise budget of $\mathrm{NEN}/(2\sqrt{12})$.

The final source of radiometric error is ILOS jitter synchronous with the chopping frequency. This gives rise to a spurious signal proportional to the radiance gradient, which is zero in the space and IFC views, but not in the atmospheric view. The allocation is based on the gradient of standard radiance profiles in the spectral channels (Halvorson 1994) and a synchronous jitter component of 1 μrad. (It should be noted that there are no mechanisms operating at the chopper frequency, because the chopper has multiple teeth.) This is an error source which does not fit neatly into the zero or slope categories: in the part of the radiance profile below 100 NEN, where the offset stability requirement is dominant, this error source is treated as a zero error, while in the part above 100 NEN the error is divided by the radiance and treated as a slope error. In a small number of channels with large radiance gradients this is the largest component of the slope error budget.

This completes the initial allocation to headings in the error budget. It will be ap-

parent from the discussion that some of the allocations are very uncertain at this stage, and further analysis of the likely instrument performance in certain areas is called for. However we can attempt an overall view of the shape of the budgets. The slope error budget is satisfactory. The budget is dominated by thermometry, which is as it should be for a radiometer calibrated by a black body, and the total is, as far as we can tell at this stage, within the requirements. A full channel-dependent analysis shows that even if we add the contributions linearly we still meet the 1% requirements, and come very close to meeting the 0.5% requirements in Channels $2-5$.

The zero error budget, however, is somewhat unsatisfactory. It is dominated by a contribution about which very little is known at present, and contains a number of significant contributions that are quite uncertain. Although the contributions have been added in quadrature, this can hardly be defended for some, particularly the correlated scan stray contributions. On the other hand the simplification of entering only the worst case in the table conceals the large range of sensitivities among them. Because the zero error requirement is expressed in terms of the NEN, it is most severe for channels with very large signal:noise ratios, such as 8 and 20. A full channel-dependent analysis produces a similar bottom line for these channels (1.06 NEN and 0.81 NEN) but the total is less than 0.5 NEN for two-thirds of the channels. There is also scope for refining our treatment of the zero errors, by considering the variations with time and angle over only that portion of the scan for which the signals are expected to be below 100 NEN. It is also possible that the requirement for the 'worst-case' channels can be relaxed, since they are used in the retrieval of minor constituents rather than the more critical temperature retrievals.

In summary then, this analysis has identified the significant sources of radiometric error and revealed the crucial areas which require further study if the requirements for HIRDLS are to be met, but suggests that this may well be possible for all channels.

In more general terms we can consider the consequences of this analysis for the design of infrared radiometers. There is to some extent a trade-off between slope error performance and zero error performance. Thus a completely cryogenic instrument (apart from the IFC black body) would reduce to negligible size all the terms involving the Planck function of instrument temperatures, and thus greatly reduce the zero errors, but would ruin the interchange between the Planck functions of the IFC black body, the IFC paraboloid, the scan mirror and the stray radiation entering the IFC black body which keeps the error terms in (17) and (10) so small. An instrument designed in this way would require an IFC black body with a very accurately known emissivity, whereas the emissivity is a comparatively small term in the current error budget. General conditions required for accurate radiometry in the thermal infrared are obviously good thermal stability, thermal uniformity and careful baffling so that stray radiation does not reflect around the structure. Accurate measurement of small radiances requires extremely high stability, frequent measurement of a good zero radiance, and the minimum change of instrument configuration between the zero and atmospheric radiance measurements.

References

Born M. and E. Wolf, 1980: *Principles of Optics.* 6th ed. Pergamon Press, 808pp.

Drummond J. R., J. T. Houghton, G. D. Peskett, C. D. Rodgers, M. J. Wale, J. G. Whitney and E. J. Williamson, 1980: The Stratospheric and Mesospheric Sounder on Nimbus-7. *Phil. Trans. Roy. Soc. Lond.*, **296**, 219–241.

Gille J. C. and J. J. Barnett, 1992: The High Resolution Dynamics Limb Sounder (HIRDLS) — an Instrument for the Study of Global Change. *The use of EOS for Studies of Atmospheric Physics*, J. C. Gille and G. Visconti, Eds., Elsevier, 433–450.

Gille J. C. and J. J. Barnett, 1994: HIRDLS Instrument Requiremnts Document (referred to in text as IRD). HIRDLS Project Document SC-HIR-18 19pp.

Gille J. C. and F. B. House, 1971: On the Inversion of Limb Radiance Measurements I: Temperature and Thickness. *J. of Atmos. Sci.*, **28**, 1427–1442.

Gille J. C. and J. M. Russell, 1984: The Limb Infrared Monitor of the Stratosphere — Experiment, Description and Results. *J. Geophys. Res.*, **89**, 5125–5140.

Halvorson C. M., 1994; Fiducial Atmospheric Radiance Profiles. HIRDLS Project Document SP-HIR-90A 44pp.

Richards A. G. 1995: Straylight: Estimates of Scatter and Diffraction Background Signals. HIRDLS Project Document TC-RAL-043B 71pp.

Taylor F. W., C. D. Rodgers, J. G. Whitney, S. T. Werrett, J. J. Barnett, G. D. Peskett, P. Venters, J. Ballard, C. W. P. Palmer, R. J. Knight, P. E. Morris, T. J. Nightingale and A. Dudhia, 1993: Remote Sensing of Atmospheric Structure and Composition by Pressure Modulator Radiometry from Space: The ISAMS Experiment on UARS. *J. Geophys. Res.*, **98**, 10 799–10 814.

Stratton J. A., 1941: *Electromagnetic Theory.* McGraw-Hill, 615pp.

Figure Captions

Figure 1: Schematic of Instrument Layout.

Figure 2: Schematic of Instrument Scan Pattern and In-Flight Calibration. The duration of this sequence is 66 s. Note that a space view is obtained on every elevation scan, and an extended space view covering the entire azimuth scan range is obtained after the IFC BB view.

Channel	Target Species	FWHM (cm^{-1})	FWHM (μm)	NEN ($mW\ m^{-2}sr^{-1}$)
1	N_2O, aerosol	563–588	17.01–17.76	1.2
2	CO_2	600–615	16.26–16.67	0.63
3	CO_2	610–640	15.63–16.39	0.59
4	CO_2	626–660	15.15–15.97	0.60
5	CO_2	655–680	14.71–15.27	0.43
6	aerosol	821–836	11.96–12.18	0.19
7	$CFCl_3$	835–853	11.72–11.98	0.20
8	HNO_3	860–905	11.05–11.63	0.21
9	CF_2Cl_2	915–933	10.72–10.93	0.20
10	O_3	990–1010	9.90–10.10	0.15
11	O_3	1011–1048	9.54–9.89	0.24
12	O_3	1120–1140	8.77–8.93	0.10
13	aerosol	1200–1220	8.20–8.33	0.11
14	N_2O_5	1229–1260	7.94–8.14	0.11
15	N_2O	1256–1282	7.80–7.96	0.11
16	$ClONO_2$	1278–1299	7.70–7.82	0.11
17	CH_4	1324–1369	7.30–7.55	0.12
18	H_2O	1385–1435	6.97–7.22	0.12
19	aerosol	1402–1416	7.06–7.13	0.13
20	H_2O	1422–1542	6.49–7.03	0.16
21	NO_2	1582–1634	6.12–6.32	0.11

TABLE 1: Spectral Channels and Radiometric Noise

Error Source	Zero Error (NEN)	Slope Error (%)
Error in IFC BB temp inferred from telemetry		0.19
IFC paraboloid temp error		0.02
IFC BB / paraboloid temp. difference		0.03
Deficit in IFC BB emissivity		0.15
Radiometric offset instability	0.24	0.01
Gain Stability	0.16	0.13
Spectral Calibration Error		0.01
Scan stray: Scan mirror T non-uniformity	0.17	0.01
Scan stray: (x term)	0.78	0.01
Scan stray: (y and z terms)	0.32	
Scan stray: (x' term)		0.01
Scan stray: (y' and z' terms)		0.01
Scan stray: Diffraction	0.58	0.00
Uncorrected non-linearity		0.10
Electronic offset stability	0.07	0.01
Synchronous ILOS jitter	0.11	0.18
TOTAL (root sum square)	1.08	0.35

TABLE 2. Radiometric Accuracy Budget

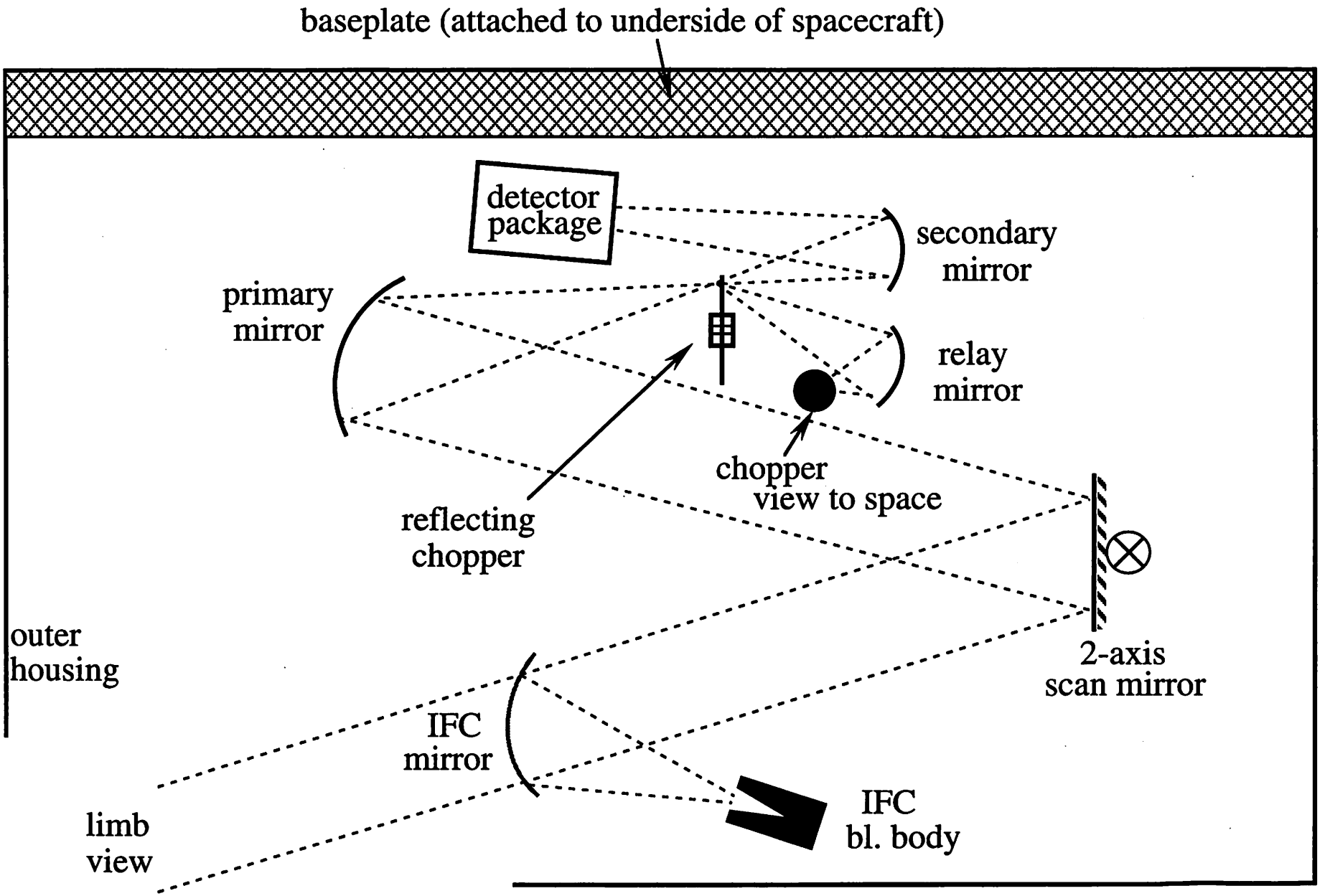
baseplate (attached to underside of spacecraft)
detector package
secondary mirror
primary mirror
relay mirror
chopper
view to space
reflecting chopper
outer housing
2-axis scan mirror
IFC mirror
IFC bl. body
limb view

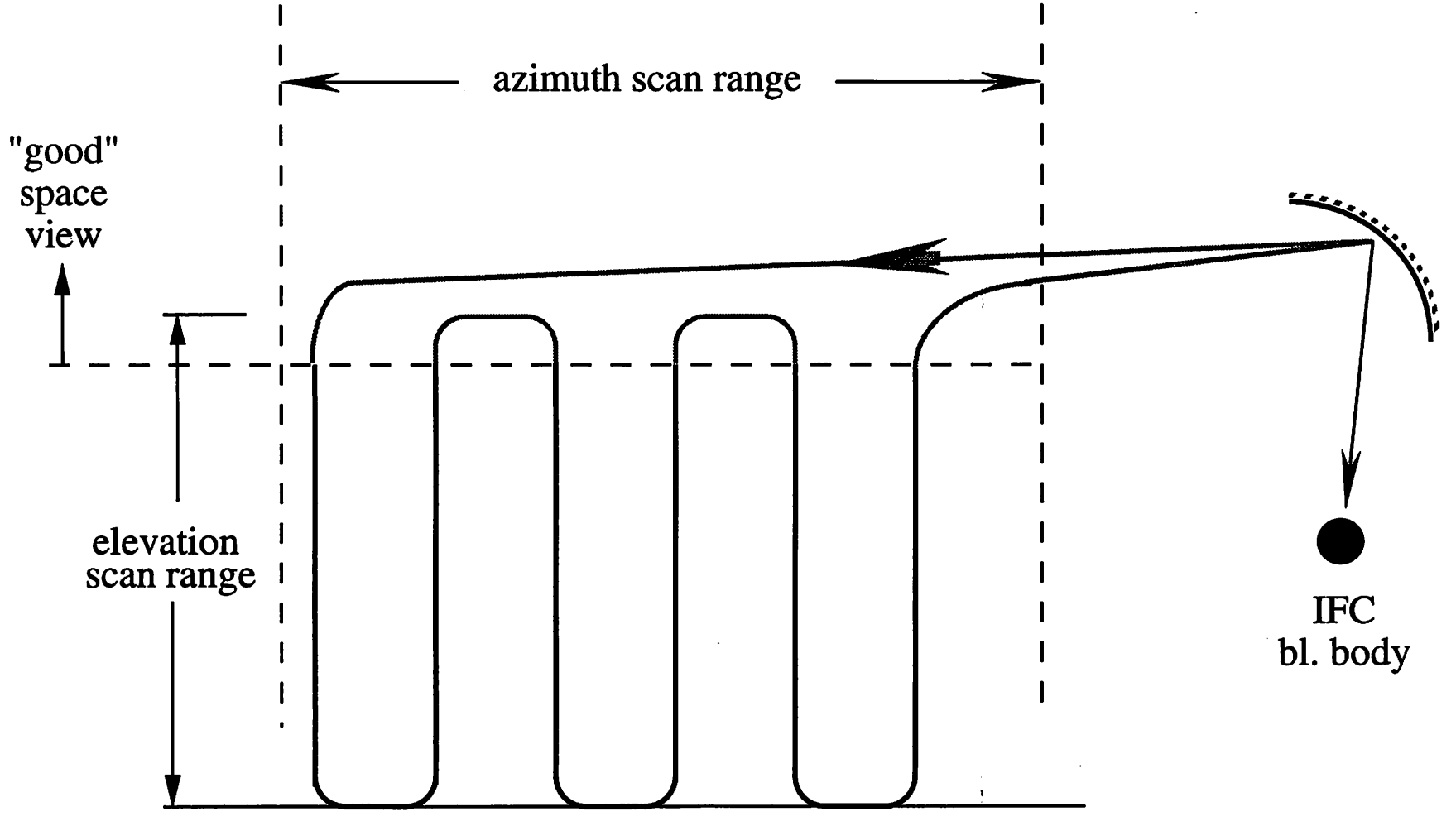
azimuth scan range
"good"
space
view
elevation
scan range
IFC
bl. body